Materials Chemistry and Physics 126 (2011) 797–803

Contents lists available at ScienceDirect

Materials Chemistry and Physics

journal homepage: www.elsevier.com/locate/matchemphys

Al and Ni co-doped ZnO films with room temperature ferromagnetism, low resistivity and high transparence

Mingpeng Yu[a], Hong Qiu[a,*], Xiaobai Chen[b], Hui Li[a], Wei Gong[a]

[a] Department of Physics, School of Applied Science, University of Science and Technology Beijing, 30 Xueyuan Road, Haidian District, Beijing 100083, China
[b] College of Mechanical Engineering, Beijing Technology and Business University, 33 Fucheng Road, Haidian District, Beijing 100048, China

ARTICLE INFO

Article history:
Received 17 June 2010
Received in revised form
20 September 2010
Accepted 13 December 2010

Keywords:
Ni and Al co-doped ZnO film
Vacuum magnetic annealing
Ferromagnetism
Resistivity
Transparence

ABSTRACT

$Zn_{0.91}Al_{0.07}Ni_{0.02}O$ and $Zn_{0.90}Al_{0.05}Ni_{0.05}O$ films of about 250 nm thick were deposited on glass substrates at 300 K by co-sputtering with ZnO:Al and Ni targets. The films were annealed in vacuum at 673 K for 2 h and then cooled down to room temperature under a magnetic field of 4.8×10^4 A m^{-1} applied along the film plane. After this process the films showed room temperature ferromagnetism, a resistivity of about 2×10^{-3} Ω cm and an average transmittance of 75% in the visible wavelength range. The films have a wurtzite structure with the *c*-axis orientation in the film growing direction and consist of thin columnar grains perpendicular to the substrate. A temperature dependence of the resistivity from 2 K to 300 K reveals that the carrier transport mechanism is thermally activated band conduction above 150 K and Mott's variable range hopping below 70 K.

1. Introduction

ZnO films co-doped with Al and transition metal (TM), as functional materials, have been intensively investigated for scientific and practical interests. Co [1–7], Ni [8–10] and Mn [3] were used as the transition metal dopants in the Al and TM co-doped ZnO films. Recently, we have prepared Al and Ni co-doped ZnO films using direct current (DC) magnetron co-sputtering and have studied their structural, electrical, optical and magnetic properties [8–10]. The Ni content in the films ranged from 4 at% to 11 at%. It was found that for the Al and Ni co-doped ZnO film the ferromagnetic behavior was enhanced by increasing Ni content. However, the optical transmittance in the visible wavelength range decreased and the resistivity increased with increasing Ni content. It is desirable to prepare Al and Ni co-doped ZnO films with high saturation magnetization, low resistivity and high transparence. While it was reported that annealing could improve the structural and physical properties of TM doped ZnO films [11–15], it has not been reported, to our best knowledge, how vacuum magnetic annealing does to the films. We report in this paper fabrication of ZnO films with above-mentioned desirable properties by vacuum annealing under magnetic field.

$Zn_{0.91}Al_{0.07}Ni_{0.02}O$ and $Zn_{0.90}Al_{0.05}Ni_{0.05}O$ films were deposited on glass substrates at 300 K by co-sputtering ZnO:Al and Ni targets. The films were annealed in vacuum under a magnetic field applied along the film plane and then were cooled down to room temperature with the magnetic field. The structure of the films was studied using X-ray diffraction (XRD), atomic force microscopy (AFM) and field emission scanning electron microscopy (FE-SEM). The magnetic, electrical, semiconducting and optical properties were measured by using a vibrating sample magnetometer (VSM), a van der Pauw method and a spectrophotometer. A magnetoresistance (MR) was measured at room temperature using a four-point probe technique. A carrier transport mechanism was discussed by measuring the temperature-dependent resistivity of the films.

2. Experimental

The DC magnetron sputtering system (KYKY Technology Development Ltd.) with two targets inclined at an angle of 45° to the same substrate has been described elsewhere in detail [16]. One target was a sintered ceramic ZnO + 2 wt%Al_2O_3 target (99.99% in purity) and the other was a Ni target (99.99% in purity) with 50 mm in diameter for both targets. The distance between the target and the substrate was about 100 mm. The glass substrates were ultrasonically rinsed in acetone, in deionized water and in ethanol. The substrate holder was rotated using a stepping motor during deposition. Prior to deposition, the working chamber was evacuated to a pressure lower than 2×10^{-4} Pa using a turbo molecular pump. A load-lock chamber was used to prevent the working chamber from air during sample transfer. About 250 nm thick Ni and Al co-doped ZnO films were deposited on glass substrates at 300 K by co-sputtering under an Ar gas (99.9995% in purity) pressure of 1 Pa. During the sputter-deposition, the sputtering power applied to the ZnO + 2 wt%Al_2O_3 target was fixed at 200 W and that applied to the Ni target was adjusted between 6 W and 8 W in order to control the Ni content in the films. According to the electron probe micro-analyzer (JEOL JXA 8100) analysis, $Zn_{0.91}Al_{0.07}Ni_{0.02}O$ and $Zn_{0.90}Al_{0.05}Ni_{0.05}O$ films were obtained. The probe current of 2.0×10^{-8} A was applied at an accelerating voltage of 20 kV with a probe diameter of about 1 μm. The deposition rate was about 0.2 nm s^{-1} and the deposition time was 20 min.

* Corresponding author. Tel.: +86 10 62333786.
E-mail address: qiuhong@sas.ustb.edu.cn (H. Qiu).

0254-0584/$ – see front matter © 2010 Elsevier B.V. All rights reserved.
doi:10.1016/j.matchemphys.2010.12.041

The $Zn_{0.91}Al_{0.07}Ni_{0.02}O$ and $Zn_{0.90}Al_{0.05}Ni_{0.05}O$ films were annealed at 673 K, which is a little higher than the Curie temperature of Ni bulk crystal (627 K), for 2 h under a vacuum of 2×10^{-3} Pa with a magnetic field of 4.8×10^4 A m^{-1}. The magnetic field was applied in the direction parallel to the surface of the films. Finally, the films were cooled down to room temperature with the magnetic field.

XRD (Rigaku Co.) was used to analyze the crystalline orientation of the films. The XRD measurements were performed in a standard θ–2θ scan using a Cu Kα radiation filtered by a crystal monochromator (wavelength $\lambda = 0.15406$ nm). The X-ray source was operated at a power of 40 kV × 200 mA. Scan speed was 0.1° s^{-1} and scan step was 0.02°. FE-SEM (Zeiss Co.) was used to observe the crystalline structure of the films. Surface smoothness and morphology of the films were investigated using AFM (Ben Yuan Ltd.).

The magnetic hysteresis loops of the films were measured at room temperature using VSM (Quantum Design Co.). The magnetic field was applied along the film plane during the VSM measurement. The magnetization data of the film was calibrated by subtracting the signal of the substrates. The resistivity and Hall's coefficient of the films were measured at room temperature using the van der Pauw method to determine carrier concentration and mobility. Metallic In was used as electrodes to form the ohmic contact. A temperature dependence of the resistivity for the films was measured in the temperature range of 2–300 K using the Cryogen-Magnet system of CFM-5T-H3-CFVTI-1.6K-24.5 with the four-point probe (Cryogenic Inc.). A magnetoresistance (MR) of the films was measured at room temperature using the Cryogen-Magnet system. During the MR measurement, the direction of the magnetic field was along the film plane and perpendicular to the direction of the measuring current. MR is defined as

$$\mathrm{MR} = \frac{R(H) - R(0)}{R(0)} \quad (1)$$

where $R(H)$ and $R(0)$ are the resistances with and without the applied magnetic field. The optical transmittance of the films was measured in the wavelength range of 300–800 nm by using the spectrophotometer of CINTRA-10E (GBC Scientific Equipment PTY Ltd.). The optical transmittance was automatically calibrated against a bare glass as a reference sample.

3. Results and discussion

3.1. Structure

Fig. 1 shows XRD patterns of the $Zn_{0.91}Al_{0.07}Ni_{0.02}O$ and $Zn_{0.90}Al_{0.05}Ni_{0.05}O$ films as-deposited and magnetically annealed. As can be seen from Fig. 1, the XRD patterns show mainly a

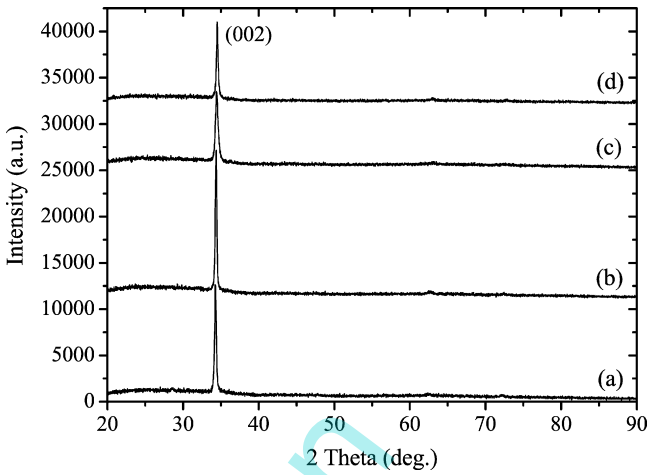

Fig. 1. XRD patterns of the Ni and Al co-doped ZnO films: (a) $Zn_{0.91}Al_{0.07}Ni_{0.02}O$ film, as-deposited, (b) $Zn_{0.91}Al_{0.07}Ni_{0.02}O$ film, annealed, (c) $Zn_{0.90}Al_{0.05}Ni_{0.05}O$ film, as-deposited, and (d) $Zn_{0.90}Al_{0.05}Ni_{0.05}O$ film, annealed.

ZnO(0 0 2) diffraction peak of hexagonal wurtzite, meaning that the films have the *c*-axis orientation perpendicular to the substrate. No other phases such as Ni, Al and their oxides can be detected in the films. After magnetically annealing, the intensity of diffraction peak increases and the peak width narrows, indicating that the crystal quality of the film is improved by annealing. The peak intensity weakens and the peak width broadens with increasing Ni content. It indicates that increase in the Ni content degrades the crystal quality of the film. It is considered that Ni atoms as an impurity influence the crystal quality of the Al and Ni co-doped films during film growing. The average crystallite sizes D can be estimated by Scherrer's formula

$$D = \frac{0.89\lambda}{\beta \cos\theta} \quad (2)$$

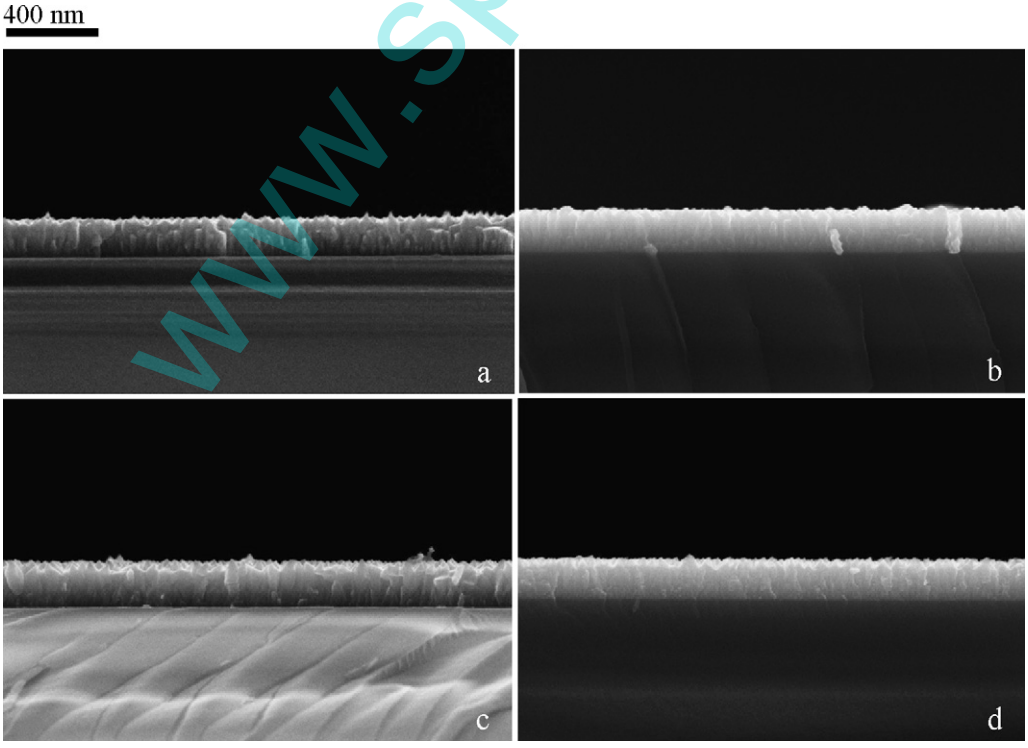

Fig. 2. Cross-sectional FE-SEM microphotographs of the Ni and Al co-doped ZnO films: (a) $Zn_{0.91}Al_{0.07}Ni_{0.02}O$ film, as-deposited, (b) $Zn_{0.91}Al_{0.07}Ni_{0.02}O$ film, annealed, (c) $Zn_{0.90}Al_{0.05}Ni_{0.05}O$ film, as-deposited, and (d) $Zn_{0.90}Al_{0.05}Ni_{0.05}O$ film, annealed.

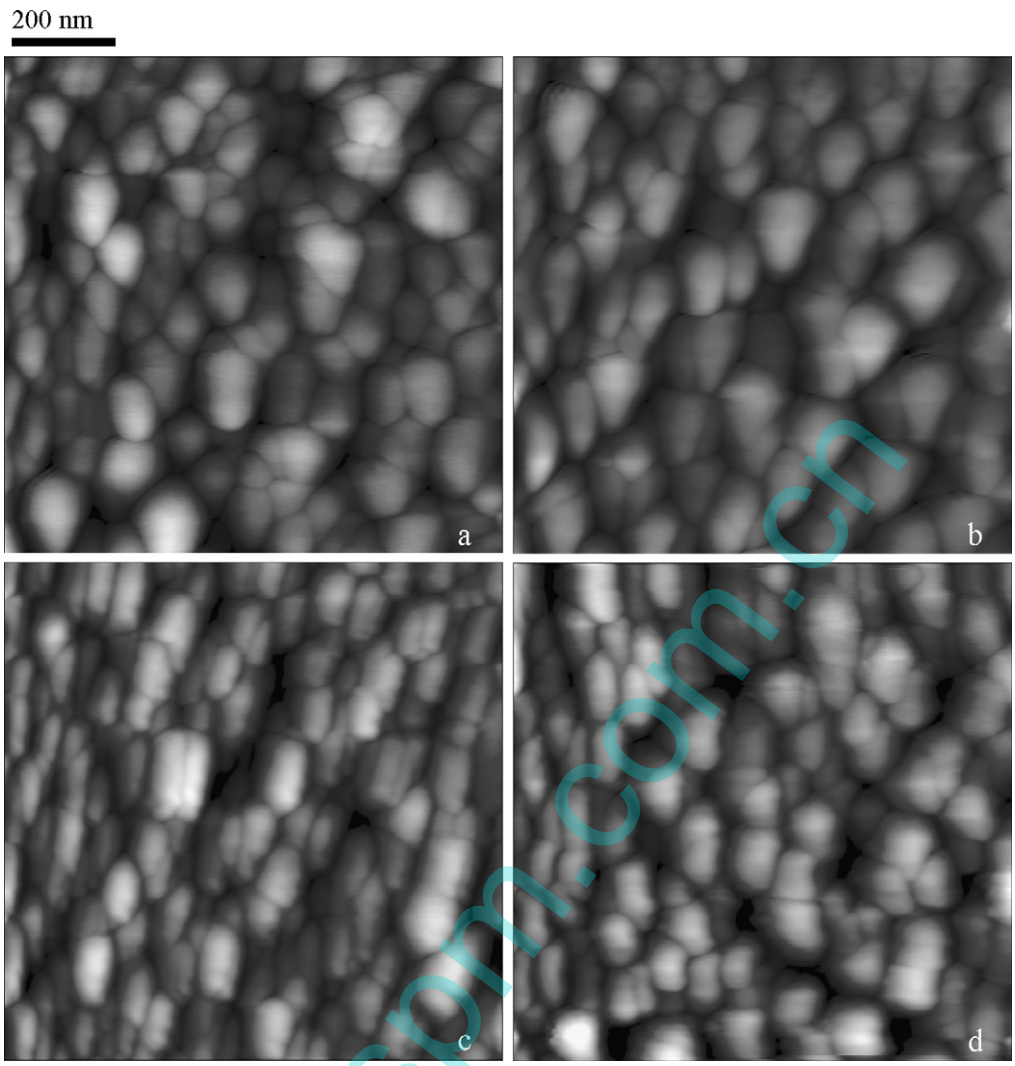

Fig. 3. AFM images of the Ni and Al co-doped ZnO films: (a) $Zn_{0.91}Al_{0.07}Ni_{0.02}O$ film, as-deposited, (b) $Zn_{0.91}Al_{0.07}Ni_{0.02}O$ film, annealed, (c) $Zn_{0.90}Al_{0.05}Ni_{0.05}O$ film, as-deposited, and (d) $Zn_{0.90}Al_{0.05}Ni_{0.05}O$ film, annealed.

where λ is the X-ray wavelength (0.15406 nm), β is the (0 0 2) full-width at half-maximum intensity and θ is the Bragg angle. The grain sizes of the as-deposited $Zn_{0.91}Al_{0.07}Ni_{0.02}O$ and $Zn_{0.90}Al_{0.05}Ni_{0.05}O$ films are calculated to be about 37 nm and 23 nm. After magnetic annealing, they increased to 41 nm and 35 nm, respectively. Furthermore, the grain size decreases with increasing the Ni content.

Fig. 2 shows cross-sectional FE-SEM microphotographs of the $Zn_{0.91}Al_{0.07}Ni_{0.02}O$ and $Zn_{0.90}Al_{0.05}Ni_{0.05}O$ films as-deposited and magnetically annealed. As can be seen from Fig. 2, all the films grow with thin columnar grains perpendicular to the substrate. The films annealed have a denser structure compared with those as-deposited. Fig. 3 shows AFM images of the $Zn_{0.91}Al_{0.07}Ni_{0.02}O$ and $Zn_{0.90}Al_{0.05}Ni_{0.05}O$ films as-deposited and magnetically annealed. As shown in Fig. 3, the films annealed exhibit a larger grain size relative to those as-deposited. The $Zn_{0.91}Al_{0.07}Ni_{0.02}O$ film has a larger grain size compared with the $Zn_{0.90}Al_{0.05}Ni_{0.05}O$ film. These results are consistent with the XRD results. Moreover, the annealing leads to an increase in the film surface roughness from 6.0 nm to 9.2 nm for the $Zn_{0.91}Al_{0.07}Ni_{0.02}O$ film and from 9.3 nm to 14.2 nm for the $Zn_{0.90}Al_{0.05}Ni_{0.05}O$ film, respectively.

3.2. Magnetic properties

For the as-deposited $Zn_{0.91}Al_{0.07}Ni_{0.02}O$ and $Zn_{0.90}Al_{0.05}Ni_{0.05}O$ films, a ferromagnetic behavior was not observed at room temperature using VSM because of a low Ni content in the films. It was reported that the Al and Ni co-doped films sputter-deposited at 300 K did not exhibit the room temperature ferromagnetism when the Ni content was lower than 10 at% [8,9].

Fig. 4 shows magnetic hysteresis loops of the $Zn_{0.91}Al_{0.07}Ni_{0.02}O$ and $Zn_{0.90}Al_{0.05}Ni_{0.05}O$ films magnetically annealed, in which the magnetic field is applied parallel or perpendicular to the direction of the annealing magnetic field during the VSM measurements. As shown in Fig. 4, the films magnetically annealed exhibit room temperature ferromagnetism. The $Zn_{0.90}Al_{0.05}Ni_{0.05}O$ film has a higher saturation magnetization and a larger coercivity compared with the $Zn_{0.91}Al_{0.07}Ni_{0.02}O$ film. The saturation magnetizations of the films are smaller than that of the Ni bulk (0.6 μ_B/Ni). The magnetic moment per Ni atom at room temperature for the $Zn_{0.90}Al_{0.05}Ni_{0.05}O$ film magnetically annealed reaches 0.1 μ_B, which is near the best value (0.14 μ_B) of the $Zn_{0.85}Al_{0.04}Ni_{0.11}O$ film grown at 573 K [9,10]. Furthermore, all the films exhibit an anisotropic magnetization behavior. The saturation magnetization

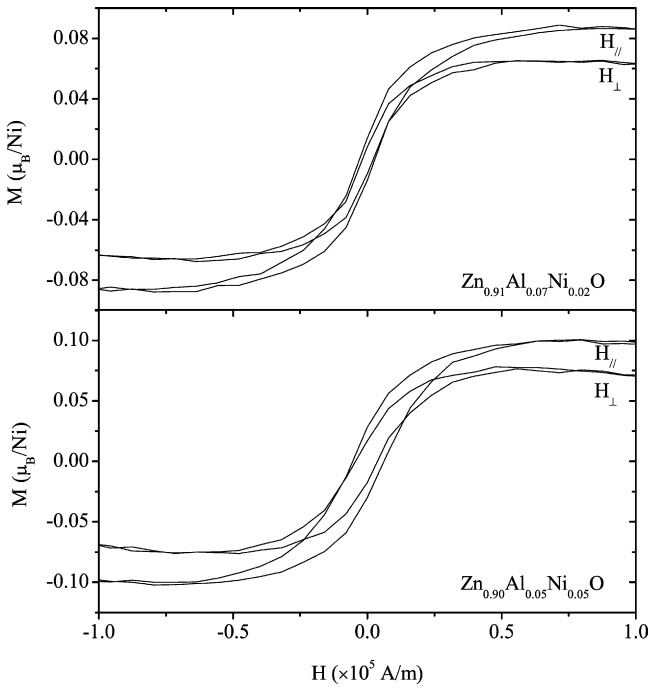

Fig. 4. Magnetic hysteresis loops of the $Zn_{0.91}Al_{0.07}Ni_{0.02}O$ and $Zn_{0.90}Al_{0.05}Ni_{0.05}O$ films magnetically annealed. $H_{//}$ and $H_{\perp}$ are the magnetic fields parallel and perpendicular to the direction of the annealing magnetic field.

and residual magnetization at a measuring field parallel to the annealing field are larger than those at a measuring field perpendicular to the annealing field. It indicates that some magnetic moments align easily along the direction of the annealing magnetic field. When the magnetic field is applied along the direction of the annealing field, the magnetic moments rotate easily to the direction of the measuring field. However, when the magnetic field is applied perpendicular to the direction of the annealing field, some magnetic moments such as those along the annealing magnetic field could not rotate to the direction of the measuring field. As a result, the films exhibit the anisotropic magnetization behavior.

Our previous work reported that the metallic Ni clusters contribute mainly to the room temperature ferromagnetism of the

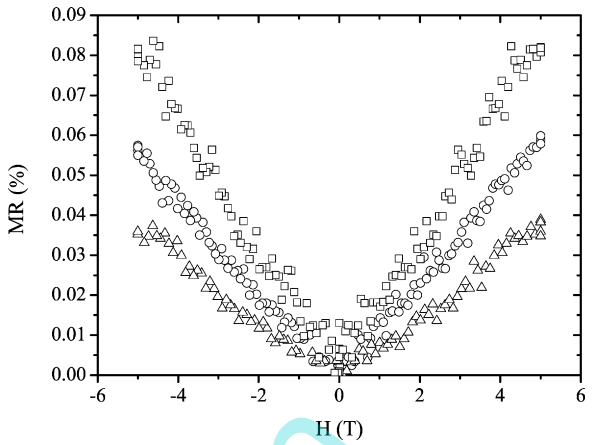

Fig. 6. Room temperature MR curves for the Al and Ni co-doped films; (□) $Zn_{0.91}Al_{0.07}Ni_{0.02}O$ film, as-deposited, (○) $Zn_{0.90}Al_{0.05}Ni_{0.05}O$ film, as-deposited, and (△) $Zn_{0.91}Al_{0.07}Ni_{0.02}O$ film, annealed.

Al and Ni co-doped films [10]. Therefore, it is considered that the room temperature ferromagnetism of the $Zn_{0.91}Al_{0.07}Ni_{0.02}O$ and $Zn_{0.90}Al_{0.05}Ni_{0.05}O$ films magnetically annealed is attributed to the Ni clusters although they are too small to be detected by XRD. Fig. 5 shows magnetic force microscope (MFM) images of the $Zn_{0.90}Al_{0.05}Ni_{0.05}O$ films as-deposited and magnetically annealed. MFM images were recorded using CSPM5000 (Ben Yuan Ltd.) at a lift height of 150 nm. As shown in Fig. 5, stripe-like domains appear for the film magnetically annealed whereas no domain structure is observed for the film as-deposited. The domain structure is attributed to the formation of the Ni clusters. Therefore, it is considered that the magnetic annealing could promote the growth of Ni clusters in the Al and Ni co-doped ZnO films, resulting in the room temperature ferromagnetism of the films.

Fig. 6 shows room temperature MR curves for the $Zn_{0.91}Al_{0.07}Ni_{0.02}O$ and $Zn_{0.90}Al_{0.05}Ni_{0.05}O$ films as-deposited and magnetically annealed. The $Zn_{0.90}Al_{0.05}Ni_{0.05}O$ film magnetically annealed did not exhibit MR behavior while the other ones have a positive MR. As it is well known, for a granular film consisting of ultrafine magnetic clusters in a non-magnetic matrix, the negative MR is attributed to spin-dependent scattering at the interface between the magnetic clusters and the non-magnetic

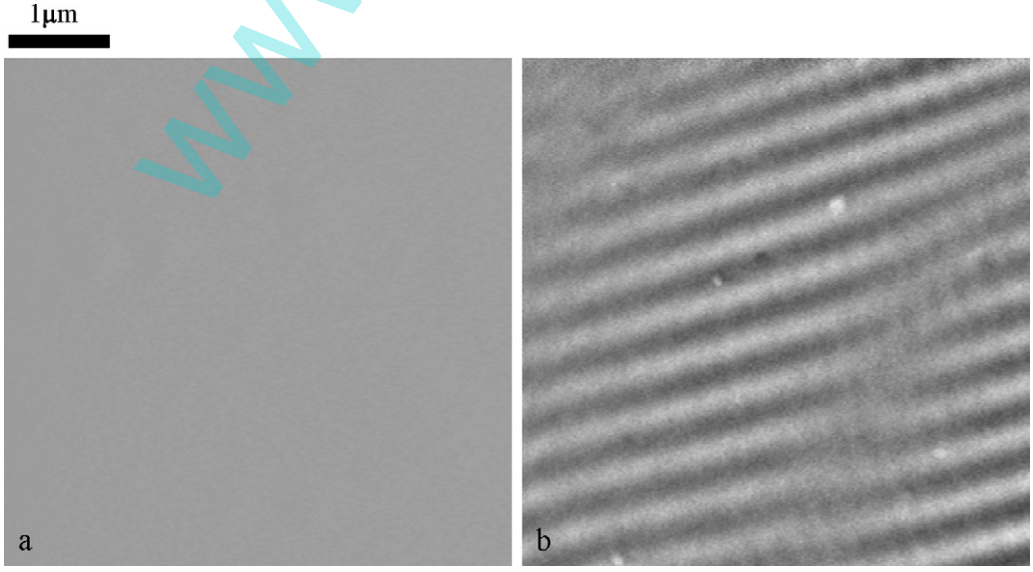

Fig. 5. MFM images of the $Zn_{0.90}Al_{0.05}Ni_{0.05}O$ films: (a) as-deposited, (b) magnetically annealed.

Table 1
The resistivities ρ, the electron concentrations n and the Hall mobilities μ of the Al and Ni co-doped ZnO films.

Film	ρ (Ω cm)	n (cm^{-3})	μ (cm^2 V^{-1} s^{-1})
As-deposited $Zn_{0.91}Al_{0.07}Ni_{0.02}O$	1.28×10^{-2}	1.13×10^{20}	4.32
As-deposited $Zn_{0.90}Al_{0.05}Ni_{0.05}O$	1.51×10^{-2}	1.54×10^{20}	2.74
Annealed $Zn_{0.91}Al_{0.07}Ni_{0.02}O$	1.98×10^{-3}	2.44×10^{20}	12.94
Annealed $Zn_{0.90}Al_{0.05}Ni_{0.05}O$	2.48×10^{-3}	2.34×10^{20}	10.73

matrix [17,18]. On the other hand, for a diluted magnetic semiconductor such as ZnO films doped with transition metals, the positive MR can be due to the s-d exchange interaction between the conducting electron and the localized spin of transition metal ion [19,20]. In the present work, it is considered that the films contain the metallic Ni (Ni clusters) and the Ni^{2+} ions in the ZnO lattice [10]. Therefore, the MR is attributed to a total effect of both the spin-dependent scattering and the s-d exchange interaction. A competition between both of them determines whether the MR is positive or negative. For the $Zn_{0.91}Al_{0.07}Ni_{0.02}O$ and $Zn_{0.90}Al_{0.05}Ni_{0.05}O$ films as-deposited, the positive MR indicates that more Ni^{2+} ions exist in the films. As a result, the films could not exhibit the room temperature ferromagnetism. After the films are magnetically annealed, the Ni clusters grow and an amount of the Ni^{2+} ions decreases, leading to a disappearance of the MR or a decrease in the positive MR. As the Ni clusters grow, the films magnetically annealed exhibit the room temperature ferromagnetism as shown in Fig. 4.

3.3. Electrical properties

All the films are n-type semiconductor. The resistivity, free electron concentration and the Hall mobility are summarized in Table 1. As shown in Table 1, annealing mainly increases the Hall mobility in the films. As a result, annealing decreases markedly the resistivity of the films. The films annealed have a resistivity of about 2×10^{-3} Ω cm, which is lower than the resistivity of the Al and Ni co-doped ZnO films previously reported [8,9]. For the Al-doped ZnO films, the Zn interstitial atoms, the O vacancies and the Al substitutional atoms in the Zn lattice sites contribute to donors [21]. Generally, it is considered that Ni^{2+} ions substitute for the Zn^{2+} ions in the Ni-doped ZnO film [15,22] and the doping of Ni does not contribute to the increase in the carrier concentration for the Ni-doped ZnO films.

Fig. 7 shows a temperature dependence of the resistivity for the $Zn_{0.91}Al_{0.07}Ni_{0.02}O$ and $Zn_{0.90}Al_{0.05}Ni_{0.05}O$ films as-deposited and magnetically annealed. As shown in Fig. 7, the resistivity of the films

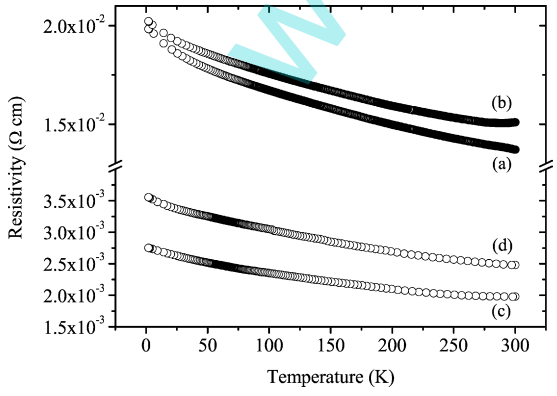

Fig. 7. A temperature dependence of the resistivity for the Ni and Al co-doped ZnO films: (a) $Zn_{0.91}Al_{0.07}Ni_{0.02}O$ film, as-deposited, (b) $Zn_{0.90}Al_{0.05}Ni_{0.05}O$ film, as-deposited, (c) $Zn_{0.91}Al_{0.07}Ni_{0.02}O$ film, annealed, and (d) $Zn_{0.90}Al_{0.05}Ni_{0.05}O$ film, annealed.

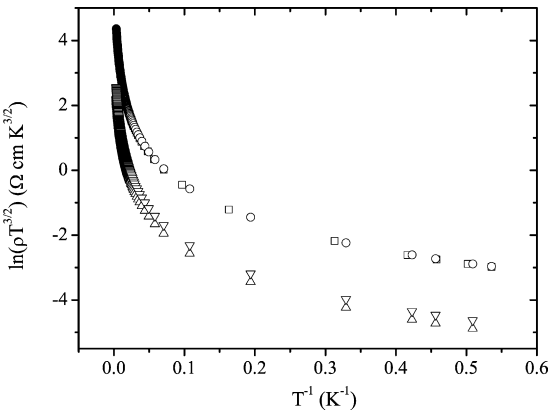

Fig. 8. A variation of $\ln(\rho T^{3/2})$ with T^{-1}: (□) $Zn_{0.91}Al_{0.07}Ni_{0.02}O$ film, as-deposited, (○) $Zn_{0.90}Al_{0.05}Ni_{0.05}O$ film, as-deposited, (△) $Zn_{0.91}Al_{0.07}Ni_{0.02}O$ film, annealed, and (▽) $Zn_{0.90}Al_{0.05}Ni_{0.05}O$ film, annealed.

decreases with increasing temperature. It exhibits a semiconducting behavior. Firstly, it is considered that for the ZnO-based films the free electron mobility is dominated by the ionized impurity scattering [10,23]. Then the resistivity ρ of the film is expressed as [24–26]

$$\rho \propto T^{-3/2} \exp\left(\frac{\Delta E_A}{kT}\right) \quad (3)$$

where T is the absolute temperature. ΔE_A is the activation energy and k is the Boltzmann constant. According to Eq. (3), for all the films, a variation of $\ln(\rho T^{3/2})$ with T^{-1} is plotted in Fig. 8. As can be seen from Fig. 8, a slope at the each point of the plots exhibits a negative activation energy. It indicates that the ionized impurity scattering could not dominate the free electron transport in the films. Secondly, it is considered that the free electron mobility is dominated by the lattice vibration scattering. The resistivity ρ of the film is given by [24–26]

$$\rho \propto T^{3/2} \exp\left(\frac{\Delta E_A}{kT}\right) \quad (4)$$

According to Eq. (4), for all the films, a variation of $\ln(\rho T^{-3/2})$ with T^{-1} is plotted in Fig. 9. As can be seen from Fig. 9, the plot cannot exhibit the linear relationship in the temperature range of 2–300 K, meaning that the free electron transport is not dominated by the single scattering mechanism. It is generally considered that the lattice vibration scattering is predominant at the relatively high temperature. As shown in the inset of Fig. 9, a good linear

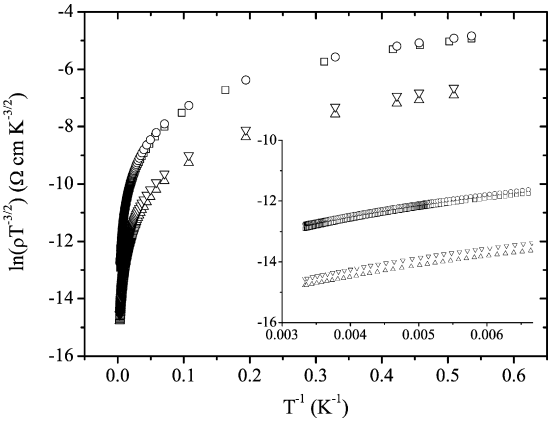

Fig. 9. A variation of $\ln(\rho T^{-3/2})$ with T^{-1}: (□) $Zn_{0.91}Al_{0.07}Ni_{0.02}O$ film, as-deposited, (○) $Zn_{0.90}Al_{0.05}Ni_{0.05}O$ film, as-deposited, (△) $Zn_{0.91}Al_{0.07}Ni_{0.02}O$ film, annealed, and (▽) $Zn_{0.90}Al_{0.05}Ni_{0.05}O$ film, annealed. The inset represents the data in the 150–300 K.

Table 2
The activation energies E_A, T_0 data, σ_0 data, the densities of localized states $N(E_F)$ and the inverse localization lengths α of the Al and Ni co-doped films.

Film	E_A (meV)	T_0 (K)	σ_0 (S cm^{-1} K$^{1/2}$)	$N(E_F)$ (cm^{-3} eV^{-1})	α (cm^{-1})
As-deposited $Zn_{0.91}Al_{0.07}Ni_{0.02}O$	34	145	970	6.6×10^{19}	3.8×10^{5}
As-deposited $Zn_{0.90}Al_{0.05}Ni_{0.05}O$	36	150	880	5.0×10^{19}	3.4×10^{5}
Annealed $Zn_{0.91}Al_{0.07}Ni_{0.02}O$	31	175	7230	3.0×10^{22}	3.1×10^{6}
Annealed $Zn_{0.90}Al_{0.05}Ni_{0.05}O$	32	185	5730	1.5×10^{22}	2.5×10^{6}

dependence having a linearity factor better than 0.990 is exhibited in the range of 150–300 K. The activation energies are calculated by the slopes of the fitted straight lines and are summarized in Table 2. They are comparable to the 25–60 meV activation energy previously reported for shallow donor levels in ZnO and ZnO:Al [25–29]. For the low temperatures below 70 K, the plots shown in Fig. 9 also exhibit a good linear dependence. The fitted activation energies are lower than 10 meV, which are smaller than the data reported. It means that the carrier transport mechanism at the low temperature is not thermally activated band conduction for the $Zn_{0.91}Al_{0.07}Ni_{0.02}O$ and $Zn_{0.90}Al_{0.05}Ni_{0.05}O$ films.

At low temperatures the carrier transport mechanism can be explained using the variable range hopping (VRH) model proposed by Mott. The electrons hop between the localized states. These localized states exist inside the energy distribution region of the impurity level in the energy gap. The electron hops from the occupied localized state to the unoccupied one under the favorable condition. In the Mott's VRH model, a relationship between the conductivity σ and the temperature T is given by [25,30–32]

$$\sigma = \sigma_0 T^{-1/2} \exp\left[-\left(\frac{T_0}{T}\right)^{1/4}\right] \quad (5)$$

where σ_0 and T_0 are expressed as

$$\sigma_0 = \frac{3e^2 \nu_P}{\sqrt{8\pi}} \times \left[\frac{N(E_F)}{\alpha kT}\right]^{1/2} \quad (6)$$

$$T_0 = \frac{16\alpha^3}{kN(E_F)} \quad (7)$$

where ν_P is the phonon frequency ($\approx 10^{13}$ Hz) at Debye's temperature. $N(E_F)$ is the density of the localized electron states at Fermi's level. α is the inverse localization length of wave function associated with the localized state. Fig. 10 shows a temperature dependence of the conductivity for the $Zn_{0.91}Al_{0.07}Ni_{0.02}O$ and $Zn_{0.90}Al_{0.05}Ni_{0.05}O$ film, plotted as $\ln(\sigma T^{1/2})$ versus $T^{-1/4}$ within 2–70 K. As can be seen from Fig. 10, the plots exhibit a good linear dependence having a linearity factor of 0.990. According to Eq. (5), the values of T_0 are calculated by the slopes of the fitted straight lines and those of σ_0 are obtained by the intercepts of the fitted lines and the $\ln(\sigma T^{1/2})$ axis. They are listed in Table 2. Using the data of T_0 and σ_0, both $N(E_F)$ and α are calculated using Eqs. (6) and (7) and are also summarized in Table 2. These data are comparable to those previously reported for the $Zn_{0.85}Al_{0.04}Ni_{0.11}O$ and ZnO:Al films [10,23]. As shown in Table 2, the films magnetically annealed have a higher density of the localized electron state and a narrower localization length of the wave function compared with those as-deposited. For the annealed $Zn_{0.91}Al_{0.07}Ni_{0.02}O$ and $Zn_{0.90}Al_{0.05}Ni_{0.05}O$ films, the high crystal quality results in the high free electron concentration and density of the localized state as well as the narrow localization length of the wave function. Finally, the carrier transport mechanism in the $Zn_{0.91}Al_{0.07}Ni_{0.02}O$ and $Zn_{0.90}Al_{0.05}Ni_{0.05}O$ films is Mott's variable range hopping in the temperature range below 70 K and thermally activated band conduction above 150 K.

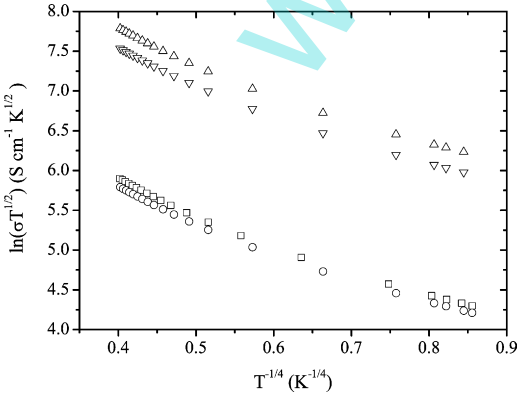

Fig. 10. A variation of $\ln(\sigma T^{1/2})$ with $T^{-1/4}$ within 2–70 K; (□) $Zn_{0.91}Al_{0.07}Ni_{0.02}O$ film, as-deposited, (○) $Zn_{0.90}Al_{0.05}Ni_{0.05}O$ film, as-deposited, (△)$Zn_{0.91}Al_{0.07}Ni_{0.02}O$ film, annealed, and (▽) $Zn_{0.90}Al_{0.05}Ni_{0.05}O$ film, annealed.

3.4. Optical properties

Fig. 11 shows optical transmittance spectra of the $Zn_{0.91}Al_{0.07}Ni_{0.02}O$ and $Zn_{0.90}Al_{0.05}Ni_{0.05}O$ films as-deposited and magnetically annealed. As can be seen from Fig. 11, average transmittance in the visible wavelength range is around 90% for the films as-deposited. For the annealed films, the average transmittance is over 75%, which is better than the transmittance of the Al and Ni co-doped ZnO films with room temperature ferromagnetism [9]. The absorption edge of the transmittance for the films annealed shifts markedly to a short wave length, i.e., blueshift. As it is well known, in the direct transition semiconductor, a relationship between the optical absorption coefficient α and the optical energy band gap E_g can be given by

$$\alpha \propto (h\nu - E_g)^{1/2} \quad (8)$$

where h is Planck's constant and ν is the frequency of the incident photon. Inset of Fig. 11 shows the relationship between α and $h\nu$ for the optical absorption edge, plotted as α^2 versus $h\nu$. As can be seen from the inset of Fig. 11, the linear dependence of α^2 on $h\nu$

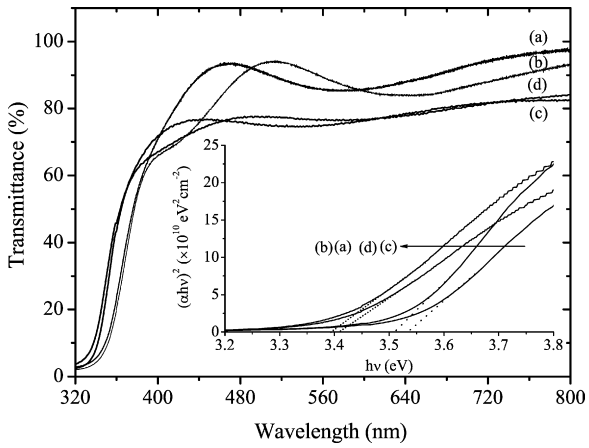

Fig. 11. Optical transmittance spectra of the Ni and Al co-doped ZnO films: (a) $Zn_{0.91}Al_{0.07}Ni_{0.02}O$ film, as-deposited, (b) $Zn_{0.90}Al_{0.05}Ni_{0.05}O$ film, as-deposited, (c) $Zn_{0.91}Al_{0.07}Ni_{0.02}O$ film, annealed, and (d) $Zn_{0.90}Al_{0.05}Ni_{0.05}O$ film, annealed. The inset represents the plots as α^2 versus $h\nu$.

indicates that the Al and Ni co-doped ZnO films are a direct transition semiconductor. The optical energy band gap E_g is obtained by extrapolating the straight portion of this plot to the photon energy axis. The E_g are determined to be about 3.4 eV and 3.5 eV for the films as-deposited and magnetically annealed, respectively. The optical energy band gap widening and the absorption edge blueshift are attributed to an increase in the carrier concentration based on the Burstein effect [33–35]. The optical results are consistent with electrical results.

4. Conclusion

The $Zn_{0.91}Al_{0.07}Ni_{0.02}O$ and $Zn_{0.90}Al_{0.05}Ni_{0.05}O$ films were sputter-deposited on glass substrates and were magnetically annealed in vacuum at 673 K for 2 h. The films have shown room temperature ferromagnetism, a resistivity of about $2 \times 10^{-3}\ \Omega$ cm and an average transmittance of 75% in the visible wavelength range. The films have a wurtzite structure with the *c*-axis orientation in the film growing direction and consist of thin columnar grains perpendicular to the substrate. A temperature dependence of the resistivity from 2 K to 300 K reveals that the carrier transport mechanism is thermally activated band conduction above 150 K and Mott's variable range hopping below 70 K. The Al and Ni co-doped ZnO films with the room temperature ferromagnetism, the low resistivity and the high transparence are successfully obtained. This functional material has potential applications in the optoelectronic and magneto-electronic devices.

Acknowledgements

The authors would like to thank Prof. J.P. He of the State Key Laboratory for Advanced Metals and Materials for FE-SEM observations. The financial supports from the Scientific Research Fund of Beijing Municipal Commission of Education Project 2009, the Fundamental Research Funds for the Central Universities 2010 and the Funding Project for Academic Human Resources Development in Institutions of Higher Learning Under the Jurisdiction of Beijing Municipality (Grant No. PHR201007122) are gratefully acknowledged.

References

[1] M. Venkatesan, P. Stamenov, L.S. Dorneles, R.D. Gunning, B. Bernoux, J.M.D. Coey, Appl. Phys. Lett. 90 (2007) 242508.
[2] L.E. Mir, Z.B. Ayadi, M. Saadoun, K. Djessas, H.J. Bardeleben, S. Alaya, Appl. Surf. Sci. 254 (2007) 570.
[3] A.J. Behan, A. Mokhtari, H.J. Blythe, D. Score, X.H. Xu, J.R. Neal, A.M. Fox, D.A. Gehring, Phys. Rev. Lett. 100 (2008) 047206.
[4] K. Samanta, P. Bhattacharya, J.G.S. Duque, W. Iwamoto, C. Rettori, P.G. Pagliuso, R.S. Katiyar, Solid State Commun. 147 (2008) 305.
[5] M. Sharma, R.M. Mehra, Appl. Surf. Sci. 255 (2008) 2527.
[6] F. Pan, C. Song, X.J. Liu, Y.C. Yang, F. Zeng, Mater. Sci. Eng. Res. 62 (2008) 1.
[7] C.L. Tsai, Y.J. Lin, C.J. Liu, L. Horng, Y.T. Shih, M.S. Wang, C.S. Huang, C.S. Jhang, Y.H. Chen, H.C. Chang, Appl. Surf. Sci. 255 (2009) 8643.
[8] T.F. Li, H. Qiu, P. Wu, M.W. Wang, R.X. Ma, Thin Solid Films 515 (2007) 3905.
[9] M.P. Yu, H. Qiu, X.B. Chen, H.X. Liu, M.W. Wang, Physica B 404 (2009) 1829.
[10] M.P. Yu, H. Qiu, X.B. Chen, H.X. Liu, Mater. Chem. Phys. 120 (2010) 571.
[11] Y.M. Cho, W.K. Choo, H. Kim, D. Kim, Y. Ihm, Appl. Phys. Lett. 80 (2002) 3358.
[12] H.S. Hsu, J.C.A. Huang, Y.H. Huang, Y.F. Liao, M.Z. Lin, C.H. Lee, J.F. Lee, S.F. Chen, L.Y. Lai, C.P. Liu, Appl. Phys. Lett. 88 (2006) 242507.
[13] N. Khare, M.J. Kappers, M. Wei, M.G. Blamire, J.L. MacManus-Driscoll, Adv. Mater. 18 (2006) 1449.
[14] B. Huang, D.L. Zhu, X.C. Ma, Appl. Surf. Sci. 253 (2007) 6892.
[15] E. Liu, P. Xiao, J.S. Chen, B.C. Lim, L. Li, Curr. Appl. Phys. 8 (2008) 408.
[16] X.B. Chen, H. Qiu, H. Qian, P. Wu, F.P. Wang, L.Q. Pan, Y. Tian, Vacuum 75 (2004) 217.
[17] A.E. Berkowitz, J.R. Mitchell, M.J. Carey, A.P. Young, S. Zhang, F.E. Spada, F.T. Parker, A. Hutten, G. Thomas, Phys. Rev. Lett. 68 (1992) 3745.
[18] J.Q. Xiao, J.S. Jiang, C.L. Chien, Phys. Rev. Lett. 68 (1992) 3749.
[19] J.H. Kim, H. Kim, D. Kim, Y.E. Ihm, W.K. Choo, Physica B 327 (2003) 304.
[20] Q. Xu, L. Hartmann, H. Schmidt, H. Hochmuth, M. Lorenz, R.S. Grund, D. Spemann, A. Rahm, M. Grundmann, Thin Solid Films 515 (2006) 2549.
[21] Y. Igasaki, H. Saito, J. Appl. Phys. 69 (1991) 2190.
[22] Z. Yin, N. Chen, F. Yang, C. Song, C. Chai, J. Zhong, H. Qian, K. Ibrahim, Solid State Commun. 135 (2005) 430.
[23] H.X. Liu, H. Qiu, X.B. Chen, M.P. Yu, M.W. Wang, Curr. Appl. Phys. 9 (2009) 1217.
[24] A. Boulouz, S. Chakraborty, A. Giani, F.P. Delannoy, A. Boyer, J. Schumann, J. Appl. Phys. 89 (2001) 5009.
[25] Y. Natsume, H. Sakata, Mater. Chem. Phys. 78 (2002) 170.
[26] A.E.J. Gonzalez, J.A.S. Urueta, R.S. Parra, J. Cryst. Growth 192 (1998) 430.
[27] D.C. Look, J.W. Hemsky, J.R. Sizelove, Phys. Rev. Lett. 82 (1999) 2552.
[28] D.C. Look, Mater. Sci. Eng. B 80 (2001) 383.
[29] P.C. Chang, J.G. Lu, Appl. Phys. Lett. 92 (2008) 212113.
[30] S. Bandyopadhyay, G.K. Paul, R. Roy, S.K. Sen, S. Sen, Mater. Chem. Phys. 74 (2002) 83.
[31] N. Brilis, D. Tsamakis, H. Ali, S. Krishnamoorthy, A.A. Iliadis, Thin Solid Films 516 (2008) 4226.
[32] R. Kumar, N. Khare, Thin Solid Films 516 (2008) 1302.
[33] E. Burstein, Phys. Rev. 93 (1954) 632.
[34] K.C. Park, D.Y. Ma, K.H. Kim, Thin Solid Films 305 (1997) 201.
[35] S.H. Jeong, J.W. Lee, S.B. Lee, J.H. Boo, Thin Solid Films 435 (2003) 78.